Positron localization in Li-Mg alloys*

P. Kubica, B. T. A. McKee, A. T. Stewart, and M. J. Stott
Department of Physics, Queen's University, Kingston, Ontario, Canada
(Received 6 June 1974)

Positron-annihilation experiments have been performed on a number of disordered Li-Mg alloys, and information on the spatial distribution of annihilating positrons has been deduced. Measurements of the angular correlation of the two annihilation γ rays and of the positron lifetime have been made and the results used to obtain core-annihilation rates. The core rate is sensitive to the distribution of the annihilating positrons between the two different sorts of sites in the alloy, and the results indicate that the positrons are sampling a much greater proportion of Li atoms in the alloy than the mean Li concentration would indicate. First-principles calculations of the positron distribution based on the positron pseudopotential are in qualitative agreement with the experimental results but do not include effects of localization. Smearing of the Fermi cutoff region of the angular correlation curve can be a measure of positron localization. Experimental results for the smearing for the dilute Li alloys indicate that the annihilating positron is localized in a region extending roughly 20 Å. It is concluded that the positron is annihilating from bound states localized to Li-rich regions of the alloy. These results are important in the interpretation of positron-annihilation experiments in disordered alloys and also in the understanding of low-lying electron states in disordered alloys.

I. INTRODUCTION

In the preceding paper by Stott and Kubica,[1] hereafter referred to as SK, a new approach was presented for describing the distribution of a thermalized positron in metals and alloys. The positron wave function for a low-lying state was factorized into a slowly varying part, termed the positron pseudo wave function, containing all the energy dependence and a prescribed core function accounting for the exclusion of the positron from the ion-core regions. Although the full product wave function is required to completely specify the spatial distribution of the positron, it is the slowly varying envelope or pseudo wave function which commands most of the interest since it reflects the affinity of the positron for one sort of cell or the other in a binary substitutional alloy. In SK the pseudopotential picture was discussed for the cases of a positron in a pure metal, in a substitutional binary alloy, and in a metal containing monovacancies. For the pure metal the positron pseudo wave function is rather flat; for the alloy it tends to be enhanced in the cells containing one type of atom, and diminished in cells containing the other type of atom, the degree of enhancement depending on the positron pseudopotential difference; at vacancies the pseudo wave function is strongly enhanced and in many cases it will be localized corresponding to a positron bound state.

Positron trapping at vacancies in some metals has been recognized for a few years.[2] Positron enhancement at one component of a substitutional alloy, leading to preferential annihilation with the electrons of those atoms, has not previously been recognized. The purpose of the work described in this paper is the investigation of positron enhancement in the Li-Mg alloy system using positron-annihilation techniques and the discussion of the results within the theoretical framework presented in SK.[3]

The positron core-annihilation rate, defined in SK as that contribution of the total annihilation rate made by annihilation with electrons in the ion-core regions, has been suggested in SK as a useful indicator of positron enhancement at one component of an alloy. The total annihilation rate (the reciprocal of the positron mean lifetime) can be obtained directly by a conventional delayed coincidence measurement of the time distribution of positrons annihilating in a sample.[4] The fraction of annihilation events which occur with electrons in the ion-core regions can be estimated in the case of simple metals from the momentum distribution of annihilating electrons. A good indication of this quantity can be obtained from the angular correlation of the annihilation γ rays.[4] The procedure for estimating this fraction is based on the separation of the angular correlation curve into two components. The first is due to annihilation with conduction electrons, outside ion-core regions, which have a "nearly free" character leading to a rather narrow, approximately parabolic component. The second component consists of a number of contributions. The core electrons have an atomic character and their higher momentum yields a broad momentum distribution. In addition, conduction-electron wave functions in the ion-core regions vary rapidly due to orthogonalization requirements, and thus also have an atomic character leading to a broad momentum distribution similar in shape but smaller in magnitude than that arising from the core electrons themselves.[5] This contribution

is included in the definition of the core annihilation rate. Other sources of high-momentum components are the spatial variation of the electron pseudo wave function and the positron wave function, but these contributions should be negligible for values of momentum considerably larger than the Fermi momentum. Thus an evaluation from angular correlation data of the fractional intensity of the broad, approximately Gaussian shaped component, provides at least an approximate measure of the fraction of annihilation events which occur with electrons in the core region having an atomic character. Multiplication of this fraction with the measured total annihilation rated yields the core annihilation rate λ_c.

The atomic character of electrons in the core region of an atom will be relatively insensitive to its environment. In particular, the core-electron wave functions and the atomic character of the valence electrons in the core region will be little changed in an alloy, although there will be small changes in the amplitude of the latter due to changes in the electron pseudo wave function. It follows that the core annihilation rate for a particular alloy concentration will be a weighted mean of the two pure metal core rates. The weighting factors are obtained from the positron pseudodensity, which provides a measure of the positron enhancement at sites of one component of the alloy.

Because of the difficulty of a first-principles calculation of annihilation rate (due largely to the uncertainty in many-body electron enhancement factors), it is convenient in discussing positron enhancement at one component of an alloy to use the reduced core rate introduced in SK. If the separate core rates in the two pure metals A and B which constitute an alloy are called λ_c^A and λ_c^B, then the reduced core rate for the AB alloy is defined as

$$\Delta\lambda_c = (\lambda_c - \lambda_c^A)/(\lambda_c^B - \lambda_c^A) , \qquad (1)$$

where λ_c is the core rate for the alloy. Experimental evaluations of the core annihilation rates for the pure metal constituents as well as for the alloys enable data to be expressed in terms of reduced core rates for comparison with theory. As emphasized in Sec. IV of SK, the reduced core rate for AB alloys will decrease linearly with the atomic fraction of A in B from the value 1 for B metal to 0 for pure A metal if the positron shows no preference for A or B sites (and neglecting volume changes on alloying). Any deviation from linearity in a reduced core rate vs atomic concentration plot will indicate a preference of the positron for either A or B sites—an enhancement of the positron pseudo wave function at the preferred atoms.

If the positron is localized in a particularly attractive region of the alloy, i.e., an impurity in a dilute alloy or a precipitate in a more concentrated alloy, this localization of the envelope of the positron wave function, the pseudo wave function, will lead to a broadening of the positron momentum distribution. If the positron is confined to a region of spatial extent Δx, then the momentum distribution will have a width of $\Delta p \approx \hbar/\Delta x$. The width of the positron momentum distribution may be detected in high-resolution angular correlation data if the positron is localized to a volume a few atomic diameters in extent. The measured total momentum distribution of the annihilating positron-electron pairs displays a sharp corner at the Fermi momentum p_F. This sharp feature is particularly prominent for the simple metals where the broad core contribution is not too large and especially at low temperatures where the thermal energy of the positron is small. It is under these conditions that the width of the positron momentum distribution due to spatial localization can be most clearly seen as a smearing of the sharp corner of the measured pair momentum distribution. This smearing can be analyzed to extract information on the extent of the localized positron wave function, as has been done by Dave *et al.*[6] in the case of positrons trapped at vacancies in metals.

The Li-Mg alloy system is in many ways ideal for an investigation of possible enhancement and localization of the positron at one component of an alloy. The calculations reported in Sec. III of SK suggest that there is a fairly large positron pseudopotential difference (0.08 Ry) between Li and Mg sites in a Li-Mg alloy, implying a relative affinity of the positron for Li sites in the alloy. Thus positron enhancement at Li sites is to be expected. In addition, both Li and Mg satisfy the practical requirement of being simple metals with rather small, easily separable, contributions from annihilation with electrons in the core regions. The core-annihilation rates for Li and Mg are also sufficiently distinct to allow a meaningful evaluation of the reduced core rate as a function of alloy composition. Of great practical importance, investigation across the whole range of Li-Mg alloy composition is possible with minimal interference from intermediate phases. The phase diagram is reproduced in Fig. 1.[7] At room temperature there is a bcc phase of up to 70-at.% Mg in Li, and an hcp phase of up to 18-at.% Li in Mg. Between 18- and 30-at.% Li is a mixed-phase region. The atomic volumes of Li and Mg differ by only 7% and there is little volume change on alloying.[8] Diffuse x-ray scattering data[9] indicate that the bcc 50-at.% alloy is an almost perfect random solution, an atom on average having 4.3 unlike nearest neighbors in comparison to 4.0 in a random, and 8.0 in an ordered, solution. The hcp alloys also differ very

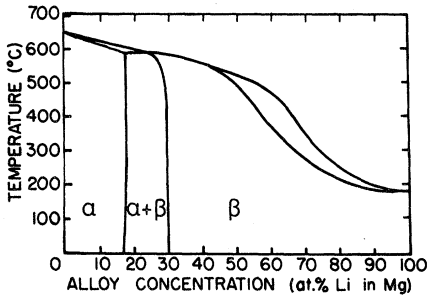

FIG. 1. Phase diagram of the Li-Mg alloy system indicating the large extent of the α and β phases.

little from random solutions. These various reasons combine to make the Li-Mg system an attractive choice for the study. It should be stressed that even if, for practical reasons, the core rate cannot be used as an indicator of positron affinity for a particular alloy system (e.g., if one constituent is a noble or transition metal), nevertheless, the positron will not sample the alloy uniformly if there is a positron pseudopotential difference between the two components.

Section II of the paper describes the preparation of the alloy specimens and the measurements of positron annihilation rate and angular correlation. The experimental results are presented in Sec. III and discussed in Sec. IV, both of these sections being subdivided into part A pertaining to positron enhancement as reflected by the core annihilation rate, and part B pertaining to positron localization as indicated by smearing of the angular correlation curve. Conclusions and implications are discussed in Sec. V.

II. EXPERIMENTAL DETAILS

The alloy specimens used in the experiments were cast from 99.9% purity Li and 99.995% purity Mg in stainless-steel tubes under a dry argon atmosphere. They were agitated while molten and after solidifying were annealed for 24 h close to the melting temperature to achieve homogeneity. Various sections of at least one ingot (1.3 cm diam$\times$8 cm length) were tested, and the alloy concentration was found to be uniform to about 0.5 at.%. Concentration of the alloys was determined by specific gravity measurement and by proton reaction analysis. The results from these two methods were in agreement to within 1 at.%. The specimens were 0.5 cm sections cut from the ingots by spark erosion. Considerable care was taken to minimize the number of lattice defects since they are potential positron traps. To obtain and maintain clean surfaces, the specimens were etched in propanol II with 0.1 to 1.0% (by volume) nitric acid added (the amount depending upon alloy concentration) and then stored in oil. The specimens were annealed in an argon atmosphere for 24 h at a temperature about 20 °C below their melting points, and a final etch was performed just prior to any measurements. These procedures yielded shiny surfaces with visible grains of average diameter about 2 mm.

The positron lifetime measurements were performed with a conventional delayed-coincidence system employing constant-fraction timing discriminators. Fairly large Pilot B plastic scintillators (4 $\times$4 cm cylinders) were used to gain efficiency. Time resolution under conditions similar to those of the measurements was 350 psec full width at half-maximum. The positron source used for these measurements was about 2 μCi of ^{22}Na deposited between two sheets of nickel foil 10^{-4} cm thick. This was in turn sandwiched between two sections of the specimen, and the whole was maintained at room temperature under vacuum during the measurements. About 2×10^6 events in the time spectra could be accumulated in 5 h counting time. The peak counts to random background ratio was 3×10^4: 1. The time scale was calibrated by a time-of-flight method using two γ-ray sources separated by 30 cm.

The measurements of the angular correlation of annihilation photons were made using "long slit" geometry. The slit width was 1.35 mm and the distance from sample to slit 2.54 m, yielding geometrical resolution of 0.53 mrad. The slits were sufficiently long (61.0 cm) that they subtended an angle in that dimension some 20 times greater than the angular width of a typical momentum distribution. The specimen was a section of an alloy ingot mounted with one flat surface in the plane of the slits. The positron source was about 100 mCi of ^{58}Co mounted above the specimen with shielding arranged so that only the specimen face was visible to the detectors. The specimen was maintained in vacuum at liquid-nitrogen temperature during measurements. Angles about 180° were scanned in 120 steps of $\frac{1}{4}$ mrad and coincidence counts were accumulated at each step for 400 sec. To reduce the effect of any electronic drift five or six scanning cycles were performed for each specimen. In three days of counting time a total of about 6×10^5 coincidence events were accumulated with 2×10^4 counts at the peak of the distribution.

III. EXPERIMENTAL RESULTS

A. Core rate

The positron lifetime data were analyzed by fitting each measured distribution to the sum of two exponential terms by a maximum likelihood criterion based on Poisson statistics. The dominant exponential term represents the main positron decay component. The second term, with less than 5%

TABLE I. Measured values of positron lifetimes and of core annihilation fractions in Li-Mg alloys. The derived core annihilation rates are also listed.

Li concentration (at.%)	τ(psec)	Core fraction (%)	Core annihilation rate (10^{-9} sec^{-1})
0	227±2	20.2±0.4	8.9±0.2
1.5	230±2	18.9±0.4	8.2±0.2
4	233±2	18.2±0.4	7.8±0.2
11	240±2	17.8±0.4	7.4±0.2
30	248±2	18.0±0.5	7.2±0.2
53	265±2	17.7±0.6	6.7±0.3
89	283.5±2	14.9±0.6	5.3±0.2
100	293±2	13.4±0.6	4.6±0.2

intensity, represents a longer-lived component and is attributed to annihilations in the source material and at surfaces. The resulting positron lifetimes deduced from the main components are listed in Table I for eight specimens; six Li-Mg alloys and pure Li and Mg. Any systematic error due to such possibilities as improper separation of the tail component would tend to affect all measurements similarly so that for comparisons between these eight measurements the statistical standard deviation of about 2 psec should be a good measure of confidence. The total annihilation rates are the reciprocals of these lifetimes.

Small adjustments were made to the angular correlation data for the same eight specimens to remove the chance coincidence background and to correct for source decay and for γ-ray absorption by the specimen. Angular correlation data normalized to equal areas for two of the specimens are shown in Fig. 2. A clear distinction can be seen between the narrow parabolic section arising from annihilation with low-momentum valence electrons and the broad, roughly Gaussian, part of the distribution. If the broad part included only events arising from annihilations with core electrons, then the fraction of these core events could be obtained exactly from the area of that part. As discussed in SK and reviewed in the Introduction, there will be other secondary contributions to the high-momentum components. One of these arises from annihilations with valence electrons in the core region and should extend to high momentum. The valence-electron wave functions in these regions will have some atomic character due to the necessary orthogonalization to the core-electron wave functions. These features will be insensitive to alloying (apart from small changes in amplitude) and should be present in the alloy as well as the pure metal. This contribution is contained in the definition of the core annihilation rate. Another of these contributions rrises from the spatial variation of the positron wave function. The pseudopotential method for the positron described in SK indicates that the shape of the positron wave function in the core region from which most of the high-momentum components arise is insensitive to alloying. A final contribution arises from annihilations with valence electrons outside the core region; the wave functions here contain high-momentum components due to scattering by the electron pseudopotential. This last contribution will be sensitive to alloying. Fortunately, it will augment the number of annihilation events in the momentum region immediately above the Fermi momentum p_F, and thus its effect on the core annihilation fraction can be minimized by fitting the high-momentum region of the angular correlation curve with a Gaussian function using a least-squares criterion beyond about $1.5p_F$. In order to clarify these different sources of high-momentum components, an orthogonal-plane-wave analysis of the pair momentum distribution is presented in an Appendix for the particular case of Li. The roles played by core electrons, the orthogonalization term in the valence-electron wave functions and the higher-plane-wave components in the valence-electron pseudo wave function are all discussed.

Figure 2 includes the lines fitted to the broad components of the two examples of angular correlation data. The reduction in the fraction of core annihilations for the 11-at.% Li alloy compared with the pure Mg result is very obvious. The core annihilation fractions and their statistical standard deviations for the eight specimens are listed in Table I. There will also be some systematic errors due to the constraint of fitting a Gaussian function and due to the inevitable inclusion of some contribution from high-momentum valence electrons. However, for comparison between the specimens

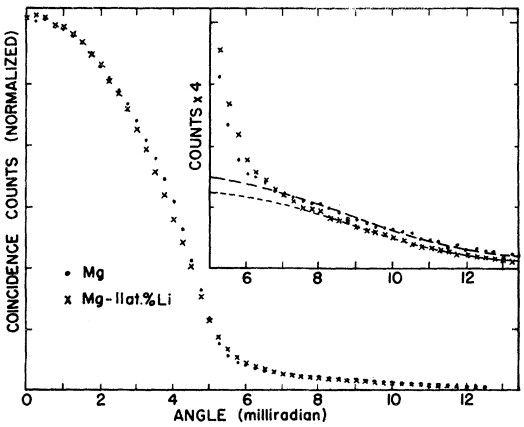

FIG. 2. Angular correlation data, normalized to equal total counts, for Mg and Mg–11-at.%-Li alloy. The results for only positive angular deviations from 180° are shown in this illustration; the full curves are symmetrical. The inset amplifies the vertical scale by a factor of 4 to yield more detail in the high-momentum region and shows the fitted Gaussian components used to obtain the core fractions.

the systematic errors should be rather similar and so the statistical uncertainties again provide a realistic measure of confidence.

The products of the total annihilation rates and the core annihilation fractions for the various specimens yield the corresponding core annihilation rates, also listed in Table I along with their standard deviations from the composite statistical uncertainties. The reduced core annihilation rates as defined in Eq. (1) are plotted in Fig. 3. The measured core rates for the two pure metals entering the expression for the reduced core rate are $\lambda_c(\mathrm{Li}) = 0.46 \times 10^9\ \mathrm{sec}^{-1}$ and $\lambda_c(\mathrm{Mg}) = 0.89 \times 10^9\ \mathrm{sec}^{-1}$.

If the positron pseudo wave function for the alloy were flat, the positron sampling the two different components merely in the ratio of their concentrations, then the reduced core rate would be a linear function of concentration between the values 1 and 0. The measured core rate can be seen in Fig. 3 to be a very nonlinear function of alloy concentration, particularly in the range of small Li concentrations; furthermore it is seen to be a concave function. The nonlinearity implies that the positron is not sampling the two components in the ratio of their concentrations and that the positron pseudo wave function is not flat but is enhanced in the core region of one component because of a positron pseudopotential difference between different sorts of sites. The concave nature of the curve implies that the positron is sampling a larger fraction of Li cores than the atomic concentration would imply; for instance, the positron would appear to be sampling Li and Mg cores in the ratio 1:2 in an alloy of mean Li concentration merely 10 at.%. This evidence supports the result of SK that the positron pseudopotential is more attractive at Li sites than at Mg sites. In Sec. IV quantitative estimates are made of the effect of the core rate of a positron pseudopotential difference between Li and Mg sites.

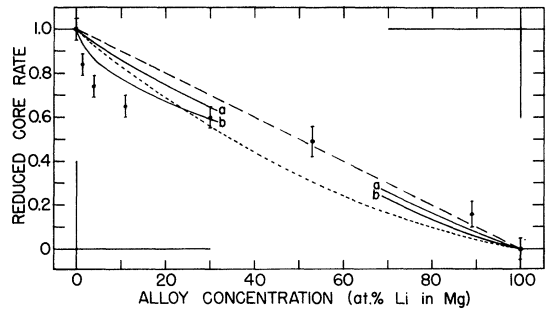

FIG. 3. Values of the reduced core annihilation rate $\Delta\lambda_c$ plotted vs alloy concentration. The error bars represent standard deviations derived from statistical uncertainties. The dashed line is straight. The two solid lines and the dotted line illustrate the results of model calculations described in the text.

B. Smearing

The angular correlation data presented in Fig. 2 show evidence of an increased blurring of the Fermi cutoff for the Mg-11-at.% Li alloy relative to that for pure Mg. This blurring is illustrated more clearly by plotting the derivative of the data, obtained directly as the difference of counts at adjacent points of the angular correlation curve.

The core component of the angular correlation curve contributes a broad, flat tail to the derivative plot. In the case of metals such as Li and Mg where the contribution from annihilations in the core regions is not large, the tail can be avoided by subtracting the broad component from the angular correlation curve before taking differences for the derivative curve. Figure 4 shows the data in derivative form for pure Mg, pure Li, and five alloys.[10] The solid line drawn in each section of the figure is a function constructed as follows:

(i) The primary ingredient is the free-electron momentum distribution corresponding to the mean valence-electron density of the sample.

(ii) This distribution is then enhanced to account for positron-electron interactions using the expression of Kahana.[11]

(iii) The enhanced momentum distribution is then convoluted with a Gaussian function chosen to simulate the smearing arising from the thermal motion of the positron and the instrumental resolution.[12]

In general, the calculated curves are in good agreement with the data; the position of the Fermi cutoff predicted by the rigid band model seems to agree with the data to a precision of about 2%, confirming the earlier results of Stewart.[13] The smearing of the data in the region of the Fermi cutoff follows the calculated curve fairly closely in the cases of the pure metals and the Li-rich alloys, but the observed smearing is considerably greater in the cases of the 4-at.% and 11-at.% Li in Mg alloys.

IV. DISCUSSION

A. Core rate

In this section the experimental results for the variation of core-annihilation rate with alloy concentration will be discussed. The pseudopotential method is used to calculate the reduced core rate using two approaches. In the first, the positron pseudodensity is estimated treating the positron pseudopotential in low-order perturbation theory. The second approach goes beyond low-order perturbation theory but is restricted in scope to a regular array of impurity atoms.

The obvious nonlinearity of the measured core rates plotted against Li concentration indicates a large enhancement of the positron pseudodensity at Li sites. Undoubtedly there are small systematic errors in the extraction of the core rates from the

raw experimental data. However, we see no way in which these uncertainties can lead to the large nonlinearity in the plot of core rate vs alloy concentration. We thus try to interpret these results in terms of the positron pseudopotential difference between Li and Mg sites in the alloy. This potential difference was estimated in SK to be 0.08 Ry for a 50-at.% alloy, the Li site being more attractive. The small variation of the potential difference with alloy concentration is neglected in our calculations. A spherical potential well of radius 3.26 a.u. and depth 0.08 Ry, corresponding to the positron pseudopotential for an isolated Li atom in Mg, has no bound state (a bound state would first appear for an unrealistically large depth of 0.23 Ry). The pseudo wave function corresponding to the lowest positron state will therefore be enhanced around the Li site, but will extend over all of the crystal. In view of this, this positron pseudodensity in the alloy can be calculated treating the pseudopotential difference within perturbation theory. It is then straightforward to estimate the reduced core rate defined by Eq. (1) using the expression obtained in SK:

$$\Delta\lambda_c = \frac{1 - \sum_{\vec{R}_A} \int_\Omega d\vec{r}\, \sigma^{\text{pseudo}}(\vec{r} - \vec{R}_A) / \int d\vec{r}\, \sigma^{\text{pseudo}}(\vec{r})}{1 + (\alpha^A/\alpha^B - 1) \sum_{\vec{R}_A} \int_\Omega d\vec{r}\, \sigma^{\text{pseudo}}(\vec{r} - \vec{R}_A) / \int d\vec{r}\, \sigma^{\text{pseudo}}(\vec{r})} , \tag{2}$$

where the summations are over the A sites $\vec{R}_A$ in the alloy, σ^{pseudo} is the positron pseudodensity, $\int_\Omega d\vec{r}$ and $\int d\vec{r}$ denote integrations over the atom cell and the whole sample, respectively, and α^A, α^B are normalization factors given by

$$\alpha^A = \int_\Omega d\vec{r}\, [U_0^A(r)]^2 ,$$

where U_0^A is the Wigner-Seitz solution for the A cell and α^B is defined similarly for the B cell.

The positron pseudo wave function is given to first order in the perturbation by

$$\psi_{\vec{k}}^{\text{pseudo}}(\vec{r}) = \frac{e^{i\vec{k}\cdot\vec{r}}}{V^{1/2}} + \sum_{\vec{q}\neq\vec{k}} \frac{\langle \vec{k}|\, V|\vec{q}\rangle}{\hbar^2 k^2/2m - \hbar^2 q^2/2m} \frac{e^{i\vec{q}\cdot\vec{r}}}{V^{1/2}} . \tag{3}$$

The perturbation is taken to be the positron pseudopotential in the alloy relative to the mean pseudopotential:

$$V(\vec{r}) = \sum_n v^{xn}(\vec{r} - \vec{R}_n) \tag{4}$$

and the matrix elements of the potential are

$$\langle \vec{k}|\, V|\vec{q}\rangle = \sum_n e^{i(\vec{q}-\vec{k})\cdot\vec{R}_n} \langle \vec{k}|\, v^{xn}|\vec{q}\rangle , \tag{5}$$

where again x denotes the sort of site either A or B in the A-B alloy.

Assuming that the position is in the $\vec{k}=0$ state when thermalized, the positron pseudodensity for a particular configuration of atoms is given by

$$\sigma^{\text{pseudo}}(\vec{r}) = |\psi_0^{\text{pseudo}}(\vec{r})|^2 . \tag{6}$$

To first order in the perturbation, this becomes merely

$$\sigma^{\text{pseudo}}(\vec{r}) = V^{-1}\left[1 - \left(\sum_{\vec{q}\neq 0} \frac{\langle 0|\, V|\vec{q}\rangle}{\hbar^2 q^2/2m} e^{i\vec{q}\cdot\vec{r}} + \text{c. c}\right)\right] . \tag{7}$$

The quantity relevant to the reduced core rate given by Eq. (2) is the fraction of the positron pseudodensity in the A-type cells. For convenience we denote this quantity by

$$\sigma_A^{\text{pseudo}} = \sum_{\vec{R}_A} \int_\Omega d\vec{r}\, \sigma^{\text{pseudo}}(\vec{r} - \vec{R}_A) \Big/ \int d\vec{r}\, \sigma^{\text{pseudo}}(\vec{r}) , \tag{8}$$

where the sum is over the A sites. From Eq. (7) we have for σ_A^{pseudo}, to first order,

$$\sigma_A^{\text{pseudo}} = C_A - \left(V^{-1} \sum_{\vec{q}\neq 0} \sum_{\vec{R}_A} \frac{\langle 0|\, V|\vec{q}\rangle}{\hbar^2 q^2/2m} \times e^{-i\vec{q}\cdot\vec{R}_A} \int_\Omega d\vec{r}\, e^{i\vec{q}\cdot\vec{r}} + \text{c. c.}\right) . \tag{9}$$

Now to make connection with experiment, the expression for σ_A^{pseudo} corresponding to a particular arrangement of the atoms must be averaged over all configurations,

$$\langle \sigma_A^{\text{pseudo}} \rangle = C_A - \left(V^{-1} \sum_{\vec{q}\neq 0} \int_\Omega d\vec{r}\, e^{i\vec{q}\cdot\vec{r}} \times \left\langle \sum_{\vec{R}_A} \sum_{\vec{R}_n} \frac{\langle 0|\, v^{xn}|\vec{q}\rangle}{\hbar^2 q^2/2m} e^{i\vec{q}\cdot(\vec{R}_n - \vec{R}_{A'})} \right\rangle + \text{c. c.}\right) . \tag{10}$$

If the alloy is assumed to be a perfect random solution, as would appear to be a good approximation for a Li-Mg alloy, then only the terms with $\vec{R}_A = \vec{R}_n$ contribute and

$$\langle \sigma_A^{\text{pseudo}} \rangle = C_A - C_A\left(\sum_{\vec{q}\neq 0} \Omega^{-1} \int_\Omega d\vec{r}\, e^{i\vec{q}\cdot\vec{r}} \frac{\langle 0|\, v^A|\vec{q}\rangle}{\hbar^2 q^2/2m} + \text{c. c.}\right) \tag{11}$$

The pseudopotential discussed in SK contains a local part and another part which depends on the gradient of the pseudo wave function. This latter part was denoted by v_G and it was argued to be small. The effect of v_G on $\langle \sigma_A^{\text{pseudo}} \rangle$ is also small, changing the reduced core rate for the dilute Li

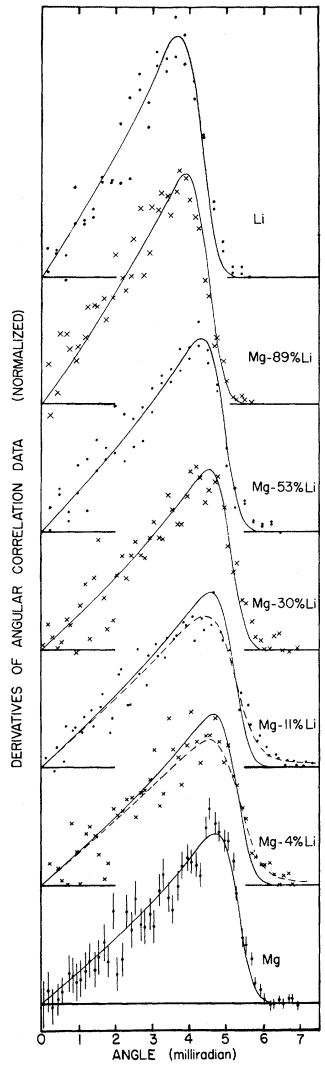

FIG. 4. Angular correlation data for Mg, Li, and five alloys shown in derivative form to emphasize the smearing in the region of the Fermi cutoff. Data for negative angular deviations from 180° have been included by folding about the centroid of the distribution. Statistical standard deviations are indicated for one set of data and are similar for the others. The solid lines are based on a free-electron model with smearing included from instrumental effects and positron temperature. The dashed line indicated in the case of two alloys includes an additional smearing component described in the text. Alloy concentrations are in at.%.

alloys by only 3%, and so it has been neglected. The only significant contribution arises from the part of the pseudopotential which is constant within an atomic cell and is given by $E_0^A + E_F^A + E_{\rm corr}^A$ within an A-type cell. The quantities E_0, E_F, and $E_{\rm corr}$ are the positron zero-point energy, the internal electron Fermi energy, and the positron-electron correlation energy, respectively. These quantities are discussed fully in SK and references giving tables of these quantities are quoted there. Replacing the atomic Wigner-Seitz cell by a sphere of radius R_a the matrix elements of the potential become

$$\langle 0 | v^A | \vec{q} \rangle = 4\pi V^{-1} \int_0^{R_a} dr\, r^2 (E_0^A + E_F^A + E_{\rm corr}^A) j_0(qr) - 4\pi V^{-1} \int_0^{R_a} dr\, r^2 [C_A (E_0^A + E_F^A + E_{\rm corr}^A) + C_B (E_0^B + E_F^B + E_{\rm corr}^B)] j_0(qr) , \quad (12)$$

where the second term arises from the mean value of the potential. Simplification of Eq. (12) yields an expression which depends on the positron pseudopotential difference V_0 between A and B cells:

$$\langle 0 | v^A | \vec{q} \rangle = \frac{3\Omega}{V} V_0 (1 - C_A) \frac{j_1(qR_a)}{qR_a} , \quad (13)$$

where

$$V_0 = E_0 + E_F + E_{\rm corr}^A - E_0^B - E_F^B - E_{\rm corr}^B .$$

Estimates of V_0 for a number of 50-at.% alloys are given in Table II of SK. Substitution of Eq. (13) into Eq. (11) leads to the final result:

$$\langle \sigma_A^{\rm pseudo} \rangle = C_A - \frac{24 m V_0 R_a^2}{\hbar^2 \pi} C_A (1 - C_A) \int_0^\infty dx \left(\frac{j_1(x)}{x} \right)^2 . \quad (14)$$

The Li-Mg psuedopotential difference from Table II of SK has the value 0.08 Ry. There is some small variation in R_a with the concentration of Li-Mg alloy, but this is neglected and an average value $R_a = 3.26$ a.u. is assumed over the whole composition range. The ratio $\alpha_{\rm Li}/\alpha_{\rm Mg}$ also enters the expression of Eq. (2) for the core rate. For Li-Mg alloys, calculations indicate that $(\alpha_{\rm Li}/\alpha_{\rm Mg} - 1) = 0.11$ and so the denominator of the expression for the reduced core rate is about unity, which value is used in the calculations. The integral in Eq. (14) can easily be evaluated numerically to yield

$$\int_0^\infty dx \left(\frac{j_1(x)}{x} \right)^2 = 0.209 .$$

The expression for the reduced core rate for Li-Mg becomes

$$\Delta\lambda_c = (1 - C_{\rm Li})(1 - 0.68\, C_{\rm Li}) \quad (15)$$

and this relationship is indicated in Fig. 3 by the dotted line.

The results of the perturbation calculation are in qualitative agreement with the measured values of core rates in that they lie below the straight line which corresponds to a positron distributed equally between the Li and Mg sites. However in the region of small Li concentrations, where the experimental points deviate most from the straight line, the calculated curve considerably underestimates

the nonlinearity of the experimental data. This indicates that the enhancement of the positron pseudodensity at the Li sites in the dilute alloy has been underestimated and the positron is actually sampling a greater fraction of Li sites than the perturbation calculation indicates. It is not impossible that the magnitude of the positron pseudopotential difference between Li and Mg cells was underestimated in SK, and so the effect of increasing the potential difference in Eq. (14) should be investigated. However, the value of V_0 used in obtaining Eq. (15), namely, -0.08 Ry, is relatively large, and the results of the first-order perturbation calculation of the positron pseudodensity must be treated with caution. A substantially larger value of $|V_0|$ used in Eq. (14) would lead to unrealistic results, particularly for the dilute alloys where the potential difference relative to the mean potential is largest.

To investigate the effect on the reduced core rate of a larger pseudopotential difference, the pseudodensity has been calculated in a way which treats well large potential differences and which should give reliable results for dilute alloys. Neglecting the small gradient part, the positron pseudopotential for an alloy consists of a potential which is constant within each cell, but has a different value in cells containing different atoms. For a dilute alloy the positron pseudo wave function in the region around one of the impurity atoms positioned at the origin should satisfy the Schrödinger equation for a potential

$$V(\vec{r}) = V_0 , \quad r < R_a$$
$$= 0 , \quad r > R_a \tag{16}$$

where V_0 is the positron pseudopotential difference and the impurity atom cell has been replaced by the sphere of equal volume. To find the wave function, the solution of the Schrödinger equation in this region must be matched to the solutions in the surrounding dilute alloy. In the perturbation calculation above it was assumed that the positron density entering the expression for the core rate was determined by the ground-state pseudo wave function alone through Eq. (16), and the same assumption is made here. By analogy with the Wigner-Seitz approximation for the $\vec{k} = 0$ valence-electron wave function the positron ground state for the potential given by Eq. (16) is taken to be the s wave which is flat at the "impurity sphere" boundary and which has no nodes within the sphere. The "impurity sphere" is the sphere which, on the average, contains one impurity and it has radius R_I given by

$$R_I = R_a C^{1/3} , \tag{17}$$

where C is the impurity concentration. Writing $E = -\hbar^2\alpha^2/2m$ and $E - V_0 = \hbar^2 k^2/2m$, where E is the positron energy, the wave function, apart from a normalization factor, is given by

$$\psi_0^{\text{pseudo}}(\vec{r}) = \frac{\sin kr}{r} , \quad r < R_a$$
$$= \frac{\sin kR_a \cosh\alpha(r - R_a) + (k/\alpha)\cos kR_a \sinh\alpha(r - R_a)}{r} , \quad R_a < r < R_I \tag{18}$$

with the boundary condition

$$\left(\frac{\partial \psi_0^{\text{pseudo}}}{\partial r}\right)_{r=R_I} = 0 .$$

The impurity may act as a potential well or barrier to the positron depending on the sign of V_0, and the validity of the approximation in no way depends upon the magnitude of V_0. It should be a good approximation when the impurities are regularly spaced, but fluctuations in the local concentration of impurities are not accounted for.

It is a simple matter to compute the pseudodensity and hence the reduced core rate from ψ_0^{pseudo}, and the relation for $\Delta\lambda_c$ as a function of Li concentration in the Li-Mg alloy system is indicated for two different values of pseudopotential difference V_0 by the full lines of Fig. 3. The cell radius R_a was taken to be 3.26 a.u. throughout the full range of composition. The curves for both values of V_0 fall below the straight line plot, indicating enhancement at Li sites as expected. However, the experimental points lie below any of the curves in the region of low Li concentration, and so the calculations underestimate the actual enhancement. The reduced core rate calculated within this model does not appear to be very sensitive to the choice of V_0, and it is inconceivable that the pseudopotential difference can be any larger in magnitude than that corresponding to curve b of Fig. 3. In fact, the largest value of $|V_0|$ chosen, 0.20 Ry, is so large (recall that the value calculated from first principles was 0.08 Ry) that an isolated impurity with this pseudopotential difference would very nearly have an actual bound state. There is a rather weak positron bound state observed at a monovacancy in Mg, [14] but the insertion into such a vacancy of a Li atom with its core, repulsive to the positron, would greatly reduce the potential well depth.

The positron pseudopotential difference between Li and Mg indicates that there will be no positron bound state around an isolated Li impurity in Mg; the positron pseudo wave function will be enhanced around the Li atom but will not be localized to it. However, if successively more Li atoms were substituted for the Mg atoms adjacent to the impurity, then eventually a cluster of Li atoms in Mg would be built up, sufficiently attractive to the positron that there would be a positron bound state. As an example consider the case of a large cluster of Li atoms in Mg amounting to a piece of Li metal in Mg. In this case the arguments used in developing the positron potential in SK indicate that the lowest positron state extending over the Li region is lower than that in the Mg region by an energy equal to the difference in the constant parts of the pseudopotential, i.e., $V_0 = 0.08$ Ry. In such a case the ground-state positron wave function would be localized to the region in and around the cluster and the contribution of Li atoms to the core rate for annihilation from this state would be totally disproportionate to the mean Li concentration. A crude estimate of the attractive strength of a cluster of Li atoms in Mg can be obtained by replacing the pseudopotential well of depth V_0 extending over a volume corresponding to n Li atoms. This approximation indicates that an isolated cluster of five or more Li atoms in Mg would bind a positron.

In the Li-Mg alloys under consideration, it is possible that the positron may be localized to exceptional regions of higher than average Li concentration. We do not mean by this merely that the positron will be trapped at isolated clusters of five or more adjacent Li atoms, but that trapping can occur in a larger region containing an excess of Li above the mean. Such an effect, which was not treated in the above calculations of core rate, would further enhance the Li contribution to the core rate. Furthermore, if the positron annihilates from states localized to regions of high local Li concentration, the spread in positron momentum resulting from the localization should be manifested in the alloy angular correlation curves as additional smearing of the Fermi cutoff over and above the smearing for pure Mg.

B. Smearing

Referring to the derivative data plotted in Fig. 4, it is evident that the smearing of the Fermi cutoff for the Mg–4-at.%-Li and Mg–11-at.%-Li alloys is in excess of the contributions from the thermal motion of the positron and the instrumental resolution which are represented by the solid lines. In view of the possibility argued above that localization of the positron might be occurring in these alloys, an additional convolution was performed on the curves represented by the solid lines to include a positron momentum distribution $P(p) = \beta^4/(p^2 + \beta^2)^2$. Such a distribution corresponds roughly to a positron bound state localized to a region of diameter $d \approx \hbar/\beta$. This additional convolution, with $\beta = 0.03$ a.u., i.e., $d \approx 20$ Å, results in a much improved fit to the experimental data for the Mg–4-at.%-Li and Mg–11-at.%-Li alloys and is indicated by the dotted lines in Fig. 4. We believe that the core-annihilation rate data together with the additional smearing of the Fermi cutoff observed for some of the Li-Mg alloys indicate that the positrons annihilating in these alloys are localized to Li-rich regions. Following is a picture, consistent with the experimental results, of the changes in the localization of positrons to be expected over the range of alloy concentration.

Li concentrations less than 1 *at.%*. The extent and number of Li-rich regions will be too small for the positron to be significantly affected, and hence there will be little or no smearing due to localization. The only experimental data in this region are those for pure Mg.

Li concentrations 1 to 30 *at.%*. In this range the Li-rich regions are sufficiently large that there are positron bound states and are sufficiently numerous for the positron to be trapped in such a localized state during its lifetime. Smearing of the pair momentum distribution arising from the positron localization will be evident.

Li concentrations greater than 30 *at.%*. As the Li concentration is increased, the Li-rich trapping regions grow in extent and the volume to which the trapped positron is confined grows in consequence. This means that the positron becomes less confined and the smearing decreases with increasing Li concentration up to 100-at.% Li.

V. CONCLUSIONS

The experimental results for the core annihilation rate for positrons in Li-Mg alloys indicate that positrons in dilute Li alloys sample a much greater proportion of Li atoms than indicated by the mean Li concentration. First-principles calculations based on the positron pseudopotential picture using perturbation theory account for the trend of the core rate with increasing Li concentration but fail to account for the magnitude of the effect. Further calculations of the core rate which are appropriate to a regular arrangement of Li atoms in the alloy but which go beyond low-order perturbation theory also fail to account for the magnitude of the effect. These results are relatively insensitive to the strength of the pseudopotential difference. Although these calculations all show enhancement of the positron wave function at Li sites, the effect of the enhancement alone is not sufficient to account for the data. We suggest that an additional effect must be considered.

Li-Mg forms a nearly random solid solution and both the calculations presented do not account properly for the disorder. In particular, the presence of localized positron states that must be present in Li-rich regions of the alloy is not treated. As discussed in Sec. IV, such Li-rich regions can localize the positron and likely account for the magnitude of the core rate. The additional experimental evidence of the smearing of the momentum distribution near the Fermi cutoff supports this picture. Thus both experimental evidence and theoretical considerations lead us to conclude that over a wide range of alloy concentration the spatial distribution of the annihilating positrons is strongly affected by localized positron states in Li-rich regions of the alloy. We believe that these conclusions are very important in the interpretation of the results of positron-annihilation experiments in disordered alloys.

A thermalized positron at room temperature will diffuse a distance ~ 1000 Å during its lifetime.[15] If it, on the average, encounters a number of vacancies, dislocations, grain boundaries, etc., and if it can loose energy sufficiently rapidly to be trapped, then the annihilating positron will sample the electron distribution in these extreme regions of the system. In a disordered alloy positrons will also tend to sample electrons in extreme regions of the alloy where the local concentration of the more attractive sort of atom is higher than average. This behavior makes the positron an unusual probe of the system; the positive muon should be similar to the positron in this respect. The results of other experiments, e.g., soft x-ray emission, optical absorption, photoemission, and electron spectroscopy for chemical analysis (ESCA) are all relatively insensitive to disorder since they sample all regions of the alloy roughly equally.

The case of positrons annihilating in ordered alloys is less complicated. The positron states will be Bloch states and the positron distribution will be periodic with a larger amplitude near one of the components of the alloy.

The conclusions drawn above about the behavior of positrons in a disordered alloy shed light on the behavior of electrons as well. They are also sensitive to the disorder. However, the electrons which are important in transport properties, the most precise probe of the electronic system, are those near the Fermi surface. These electrons have large kinetic energies and are insensitive to small fluctuations in the crystal potential due to disorder. It would be the slow electrons near the bottom of the conduction band which would be sensitive to the disordered regions, with localized electron states being manifested as a low-energy tail to the density of states. However the electronic system is a many-particle system and the density of states is not directly measurable. Experiments such as ESCA and soft x-ray emission are the simplest that yield a quantity related to a density of states, but they involve the removal of an electron from the Fermi distribution. The "hole" that remains has a finite lifetime and decays through the creation of electron-hole pairs. Such a "hole" near the bottom of the conduction band (for an electron density corresponding to Al) has a lifetime which corresponds to an energy uncertainty ≈ 1.3 eV.[16] This blurring would obscure any effects due to disorder.

In contrast there is not likely to be more than one positron in the sample at any time. The positrons that are actually sampled through the decay process are precisely those that are sensitive to the disorder, that is, those that fall down into the lowest-lying positron states. Thus these observations of positron states yield insight into the nature of low-lying electron states in a disordered alloy.

ACKNOWLEDGMENTS

We thank R. Boulton and G. Ewan for the proton reaction analysis of the alloy specimens.

APPENDIX: CORE RATE FOR Li METAL

In the Appendix the contribution of atomic features in the valence-electron wave functions for Li are investigated using OPW wave functions. The wave functions for the valence band are taken to be single OPW's, $\chi_{\vec{k}}$, which for Li have the form

$$\chi_{\vec{k}}(\vec{r}) = A(\vec{k})\left(\frac{e^{i\vec{k}\cdot\vec{r}}}{V^{1/2}} - \int d\vec{r}\,' \Phi_{\vec{k}}^{*}(\vec{r}\,')\,\frac{e^{i\vec{k}\cdot\vec{r}\,'}}{V^{1/2}}\,\Phi_{\vec{k}}(\vec{r})\right), \quad \text{(A1)}$$

where A is a normalization factor and $\Phi_{\vec{k}}$ is the tight-binding core-electron wave function given by

$$\Phi_{\vec{k}}(\vec{r}) = \frac{1}{N^{1/2}}\sum_{n}\varphi(\vec{r}+\vec{R}_n)e^{i\vec{k}\cdot\vec{R}_n}, \quad \text{(A2)}$$

with φ representing the atomic 1s orbital for Li. Simplifying Eq. (A1),

$$\chi_{\vec{k}}(\vec{r}) = \frac{A(\vec{k})}{V^{1/2}}\left(e^{i\vec{k}\cdot\vec{r}} - \tilde{\varphi}(\vec{k})\sum_{n}\varphi(\vec{r}+\vec{R}_n)e^{i\vec{k}\cdot\vec{R}_n}\right), \quad \text{(A3)}$$

where $\tilde{\varphi}(\vec{k})$ represents the Fourier transform of $\varphi(\vec{r})$ and

$$A(\vec{k}) = [1 - (N/V)|\tilde{\varphi}(\vec{k})|^2]^{-1/2}.$$

The contribution of the valence electrons to the positron-electron pair momentum distribution is given by

$$N_v(\vec{p}) = \mathcal{E}_v\sum_{k<k_F}\left|\int d\vec{r}\,\psi_+(\vec{r})\chi_{\vec{k}}(\vec{r})e^{i\vec{p}\cdot\vec{r}}\right|^2, \quad \text{(A4)}$$

where ψ_+ is the positron wave function and $\mathcal{E}_v$ is a many-body enhancement factor for annihilation with valence electrons assumed here to be momentum

independent. The corresponding contribution of the core electrons is

$$N_c(\vec{p}) = \mathcal{S}_c \sum_{\vec{k}} \left| \int d\vec{r}\, \psi_+(\vec{r})\, \Phi_{\vec{k}}(\vec{r}) e^{i\vec{p}\cdot\vec{r}} \right|^2 . \quad \text{(A5)}$$

Substitution of Eq. (A3) into Eq. (A4) yields for the valence-electron contribution to the pair momentum distribution

$$\begin{aligned} N_v(\vec{p}) = \sum_{k<k_F} \mathcal{S}_v \frac{|A(\vec{k})|^2}{V} \Big[& \left| \int d\vec{r}\, \psi_+(\vec{r}) e^{i(\vec{k}+\vec{p})\cdot\vec{r}} \right|^2 \\ & - 2\tilde{\varphi}(\vec{k}) \int d\vec{r}\, \psi_+(\vec{r}) e^{i(\vec{k}+\vec{p})\cdot\vec{r}} \\ & \times \sum_n e^{i(\vec{k}+\vec{p})\cdot\vec{R}_n} \int d\vec{r}\, \psi_+(\vec{r}) \varphi(\vec{r}) e^{i\vec{p}\cdot\vec{r}} \\ & + N |\tilde{\varphi}(\vec{k})|^2 \sum_n e^{i(\vec{k}+\vec{p})\cdot\vec{R}_n} \left| \int d\vec{r}\, \psi_+(\vec{r}) \varphi(\vec{r}) e^{i\vec{p}\cdot\vec{r}} \right|^2 \Big] . \end{aligned} \quad \text{(A6)}$$

The first term on the right of Eq. (A6) contributes little in the range $p > k_F$ since the high-momentum components in the positron wave functions are small.[17] It is this term that leads to the characteristic parabolic contribution to the angular correlation curve for long-slit geometry. The second is an interference term contributing to N_v principally again in the range $p < k_F$ because of the small high-momentum components of ψ_+. The dominant contribution for $p > k_F$ is the third term; it arises from the orthogonalization of a plane wave to the core-electron wave function, and only annihilations in the region of the ion cores contribute.

For comparison with a polycrystalline sample $N_v(\vec{p})$ must be spherically averaged. The sum in the third term then becomes

$$\left\langle \sum_n e^{i(\vec{k}+\vec{p})\cdot\vec{R}_n} \right\rangle = \sum_n e^{i\vec{k}\cdot\vec{R}_n} \frac{\sin pR_n}{pR_n}$$

and for large p because the phases are almost random only the term $n = 0$ contributes. This yields for p greater than k_F

$$\langle N_v(\vec{p}) \rangle \approx |A(0)|^2 (N^2/V) \mathcal{S}_v |\tilde{\varphi}(0)|^2 \times \left\langle \left| \int d\vec{r}\, \psi_+(\vec{r}) \varphi(\vec{r}) e^{i\vec{p}\cdot\vec{r}} \right|^2 \right\rangle \quad \text{(A7)}$$

since $\varphi(\vec{r})$ is a localized function and consequently $\tilde{\varphi}(\vec{k})$ is slowly varying.

The core-electron contribution to the pair momentum distribution from Eq. (A5) becomes

$$\langle N_c(\vec{p}) \rangle = 2N \mathcal{S}_c \left\langle \left| \int d\vec{r}\, \psi_+(\vec{r}) \varphi(\vec{r}) e^{i\vec{p}\cdot\vec{r}} \right|^2 \right\rangle . \quad \text{(A8)}$$

Inspection of Eqs. (A7) and (A8) reveals that the core-electron contribution to the pair momentum distribution and the contribution of atomic features in the valence-electron wave functions in the core region arising from orthogonality differ only by a factor which is roughly momentum independent. Choosing for the 1s orbital $\varphi(\vec{r}) = (\alpha^3/\pi)^{1/2} e^{-\alpha r}$ with $\alpha = 2.69$ for Li,[18] so that $\tilde{\varphi}(\vec{k}) = (\alpha^3/\pi)^{1/2} 8\pi\alpha / (\alpha^2 + k^2)^2$, we find $\langle N_v(\vec{p}) \rangle / \langle N_c(\vec{p}) \rangle \approx 9\%$, with $\mathcal{S}_v = 7$ (Ref. 11) and in the absence of a calculated core enhancement factor for Li the value $\mathcal{S}_c = 3$ (Ref. 19) for Na was taken. In fact $\mathcal{S}_v$ appropriate for the OPW wiggles is probably intermediate between the electron gas value of 7 and $\mathcal{S}_c$. In the case of a simple metal such as Li, mixing into the valence-electron wave functions of higher momentum OPW's should not substantially affect the pair momentum distribution in the higher-momentum range chosen for the Gaussian fitting procedure, i.e., $p > 1.5k_F$. For other simple metals with more than just a single core state to which the valence-electron wave functions must be orthogonal, similarity between the core and valence contributions to the pair momentum distribution noted for Li should persist provided the dominant contribution from the core is from the outer shell.

The analysis indicates that the broad "core" component of the angular correlation curve results from annihilation in the core regions. For Li about 90% of this arises from core electrons themselves, the bulk of the remainder from atomic features of the valence-electron wave functions.

---

*Work supported by the National Research Council of Canada.

[1]M. J. Stott and P. Kubica, preceding paper, Phys. Rev. B 11, 1 (1975).

[2]For a recent review of positron-annihilation techniques applied to the study of vacancies see A. Seeger, J. Phys. F 3, 248 (1973).

[3]A preliminary report of this work was presented at the Second International Conference on Positron Annihilation, Kingston, Ontario, Canada, 1971 (unpublished).

[4]A review of experimental techniques has been made by R. N. West, Adv. Phys. 22, 263 (1973).

[5]The magnitude depends on the electron pseudodensity in the core region. The point is discussed in Sec. III and in the Appendix.

[6]N. K. Dave, B. T. A. McKee, A. T. Stewart, M. J. Stott, and W. Triftshäuser, Proceedings of the Second International Positron Annihilation Conference, Kingston, Ontario, Canada, 1971 (unpublished), p. 4.49.

[7]M. Hansen, *Constitution of Binary Alloys* (McGraw-Hill, New York, 1958).

[8]F. H. Herbstein and B. L. Averbach, Acta Met. 4, 407 (1956).

[9]F. H. Herbstein and B. L. Averbach, Acta Met. 4, 414 (1956).

[10]The derivative data for the Mg–1.5-at.%-Li alloy is not presented because it was discovered that the sample surface was tilted.

[11]S. Kahana, Phys. Rev. 129, 1622 (1963).
[12]The full width at half-maximum of the Gaussian function was 0.7 mrad. Contributions to this width were 0.53 mrad from the finite slit width, 0.42 mrad from the positron temperature (assuming an effective mass of 2), and 0.04–0.13 mrad from the penetration profile in the sample.
[13]A. T. Stewart, Phys. Rev. 133, A1651 (1964).
[14]B. T. A. McKee (private communication).
[15]B. Bergersen, C. H. Hodges, P. Kubica, E. Pajanne, and M. J. Stott, Solid State Commun. (to be published).
[16]L. Hedin, Phys. Rev. 139, A796 (1965).
[17]See for example the table of plane-wave coefficients for the position $k = 0$ wave function for Al, P. Kubica and M. J. Stott, J. Phys. F (to be published).
[18]W. E. Duncanson and C. A. Coulson, Proc. R. Soc. Edinb. A 62, 37 (1944).
[19]J. P. Carbotte and A. Salvadori, Phys. Rev. 162, 290 (1967).